

Robust Ladder Climbing with a Quadrupedal Robot

Dylan Vogel*, Robert Baines*, Joseph Church, Julian Lotzer, Karl Werner, and Marco Hutter

Abstract—Quadruped robots are proliferating in industrial environments where they carry sensor suites and serve as autonomous inspection platforms. Despite the advantages of legged robots over their wheeled counterparts on rough and uneven terrain, they are still yet to be able to reliably negotiate ubiquitous features of industrial infrastructure: ladders. Inability to traverse ladders prevents quadrupeds from inspecting dangerous locations, puts humans in harm’s way, and reduces industrial site productivity. In this paper, we learn quadrupedal ladder climbing via a reinforcement learning-based control policy and a complementary hooked end-effector. We evaluate the robustness in simulation across different ladder inclinations, rung geometries, and inter-rung spacings. On hardware, we demonstrate zero-shot transfer with an overall 90% success rate at ladder angles ranging from 70° to 90°, consistent climbing performance during unmodeled perturbations, and climbing speeds 232× faster than the state of the art. This work expands the scope of industrial quadruped robot applications beyond inspection on nominal terrains to challenging infrastructural features in the environment, highlighting synergies between robot morphology and control policy when performing complex skills. More information can be found at the project website: <https://sites.google.com/leggedrobotics.com/climbingladders>.

I. INTRODUCTION

Historically, most quadruped robots were limited to locomotion on highly structured terrains [1]. Advances in control architectures and hardware over the past decade have resulted in systems which can perform feats of agility, including stable locomotion over irregular natural surfaces [2], [3] and “parkour”-like leaping over obstacles [4], [5]. Nowadays, due to their ability to traverse rough terrain and remain stable on uneven surfaces, quadruped robots are becoming commonplace at industrial sites where they perform routine inspection tasks in environments that are dangerous or undesirable to humans [6]. Despite ongoing advances, quadruped robots are still unable to robustly traverse many types of infrastructure that are common in man-made environments, a key example being ladders.

Ladder falls are a major occupational hazard; the American Academy of Orthopedic Surgeons estimates that 500,000 ladder-related injuries occur per year in the United States alone [7]. To minimize occupational risk and improve site efficiency, next-generation industrial inspection robots must be able to robustly negotiate all types of industrial terrain, including ladders. However, quadrupeds are not normally equipped with the appropriate morphology or control policy for such a task. Consider the following:



Fig. 1. Composite image of a quadrupedal robot equipped with hooked end-effectors, ascending a ladder in 4 s with a reinforcement learning-based control policy. Ladder shown has parameters 90° incline, 1.8 m length, 0.3 m inter-rung spacing, 2.5 cm rung radius, and 1 m width.

- Quadruped legs are usually designed with ball-shaped or flat feet which preclude the generation of anchoring forces required for reliable upward movement [8].
- The mechanics of ladder climbing involve full-body coordination to stabilize the center of mass and move upward at a high degree of inclination [9]—something that current locomotion controllers cannot accomplish reliably in unmodeled or “noisy” environments [10].
- Ladders may vary widely in total length (L_{len}), width (L_{width}), inter-rung spacing (L_{space}), rung type (flat or round), rung radius (L_{radius}), and degree of inclination (L_θ), requiring robust generalization of a controller.

Indeed, robotic ladder climbing has proven an elusive task, posing many interconnected challenges that have been the subjects of study for decades.

Previous research on robotic ladder climbing has been conducted mainly with humanoid robots, been characterized by very slow climbing speeds, and has not generalized beyond specific ladder configurations in structured environments (e.g., completely vertical ladders and no perturbations) [11]. For example, a humanoid equipped with dexterous hands and an *a priori* motion trajectory climbed a vertical ladder [12]. Further extensions of this work validated the robot on several different vertical ladders, but did not demonstrate improved speed (it was still confined to a slow pace of 26 mm/h vertical ascent) or robustness to perturbations [13]. In another work,

* Equal contribution

All authors are with ETH Zurich, Robotics Systems Lab; Leonhardstrasse 21, 8092 Zurich, Switzerland. Contact: dyvogel@ethz.ch

a motion planner and a compliance controller were combined to generate disturbance-resistant climbing trajectories, but in the one ladder example demonstrated on hardware, the robot took seven minutes to traverse only five rungs [14].

Ladder climbing has also been demonstrated with a few quadrupeds [15], [16]. Like research to-date on humanoid ladder climbing, completely vertical ladders were the only subjects of these studies. Furthermore, the robots' movements up the ladders were also slow, taking up to two minutes to ascend a single rung.

Outside of ladder climbing specifically, robust locomotion of quadrupeds has been demonstrated in other challenging environments. Model-based methods, built around non-linear model predictive control or other optimization methods, typically excel in sparse terrains such as stepping stones and gaps [17]. However, such methods are vulnerable to modeling uncertainties, external disturbances, and degraded perception. In contrast, model-free methods such as reinforcement learning (RL) have shown great simulation to reality (sim2real) transfer, real-world robustness over rough terrain [18], [2], [19], and steady progress on sparse terrain problems such as stepping stones [20], [21], [22] and parkour [5]. Even so, no work to date has addressed the need for fast, robust, and generalizable ladder climbing with quadrupedal robots.

In this paper, we address long-standing challenges in robotic ladder climbing with the following contributions:

- An RL framework for tracking position commands, enabling robust ladder climbing (Fig. 1; Supplementary Video).
- A hooked end-effector design that generates the necessary forces for secure and repeatable climbing (Fig. 2).
- Extensive simulations of successful ladder climbing across diverse configurations parameterized by L_{len} , L_{width} , L_{space} , L_{radius} , and L_θ .
- Hardware demonstrations of the fastest and most generalized robotic ladder climbing to date, tested on ladders with varying L_θ and under unmodeled perturbations.

II. METHODS

The general training process for the control policy is illustrated in Fig. 3 and follows that of reference [2]. First, in a simulation of the robot equipped with the hooked end-effectors, we train a teacher policy with access to noiseless proprioceptive observations o_p , noiseless inertial measurement unit (IMU) history o_i^H , a height scan around the robot o_e , and privileged state information s_p . The student policy is then distilled that only has access to noisy on-board proprioceptive measurements \hat{o}_p , IMU history \hat{o}_i^H , and ladder state \hat{s}_l . The resulting student policy outputs joint position targets q_i at 50 Hz, which are tracked by a PD controller running at 400 Hz on the real robot. A neural network serves to model actuation dynamics in simulation [23].

A. Policy Observations

Proprioceptive observations o_p include the commanded target position, target heading, gravity direction in base

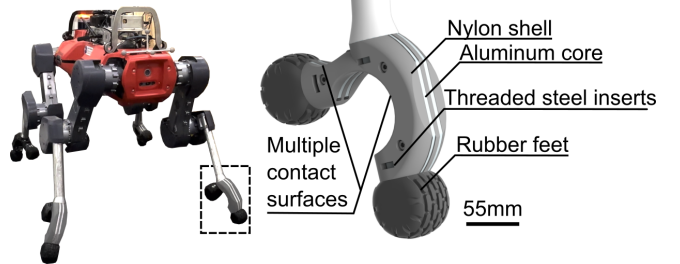


Fig. 2. Quadruped robot used for testing, equipped with four hooked end-effectors. Composed of aluminum cores and 3D printed shells, the hook design features concave surfaces that encourage stable poses on round rungs, as well as protrusions that allow the robot to push and pull on the rungs.

frame, joint positions, joint velocities, a history of joint tracking errors and velocities, a history of previous policy actions, and a binary flag indicating whether the agent is within 15 cm of the goal position. A history of the last eight IMU measurements (o_i^1, \dots, o_i^8) at 400 Hz is also provided, which includes base linear acceleration and angular velocity. Direct IMU readings are used in lieu of the base velocities output by the ANYmal state estimator, as the latter was observed to produce linear errors up to 1 m/s while climbing.

A height scan around the robot o_e with dimensions 2x1 m and a resolution of 10 cm is also input during teacher training because it helps the policy train faster. Later, o_e is removed during student training, as regions above the robot are unobservable during deployment.

Privileged state information s_p includes body contact states, contact forces at the feet, feet friction coefficients, external forces and torques applied to the base, external forces applied to the feet, mass added to the base, airtime of each foot, feet positions in base frame, a vector of the ladder state s_l , and the ladder pose p_l . The ladder state comprises a binary flag that indicates whether a ladder is present in the current terrain, ladder inclination, width, the number of rungs, rung radius, and rung spacing. The ladder pose consists of the position and yaw of the bottom rung in the robot base frame. The noisy ladder state \hat{s}_l and pose \hat{p}_l are given as observations during student training and are estimated from motion capture data during real-world deployment.

B. Teacher Policy Training

The teacher policy consists of four separate MLPs, each with elu activations (Fig. 3). Smaller MLPs first encode the height scan, privileged, and IMU observations before concatenating them with proprioceptive observations. A larger MLP then processes them into the final actions.

The teacher is trained using IPO [24] with adaptive constraint thresholding [19]. The rewards are summarized in Tab. I & II, and constraints are used to enforce the joint limits (position, velocity, torque). Episodes are terminated if the robot base inclination exceeds 100° in pitch or roll.

We randomly generate two different types of terrain for training: i) rough terrain consisting of boxes and slopes, and ii) ladders of varying L_{len} , L_θ , L_{width} , L_{space} , and

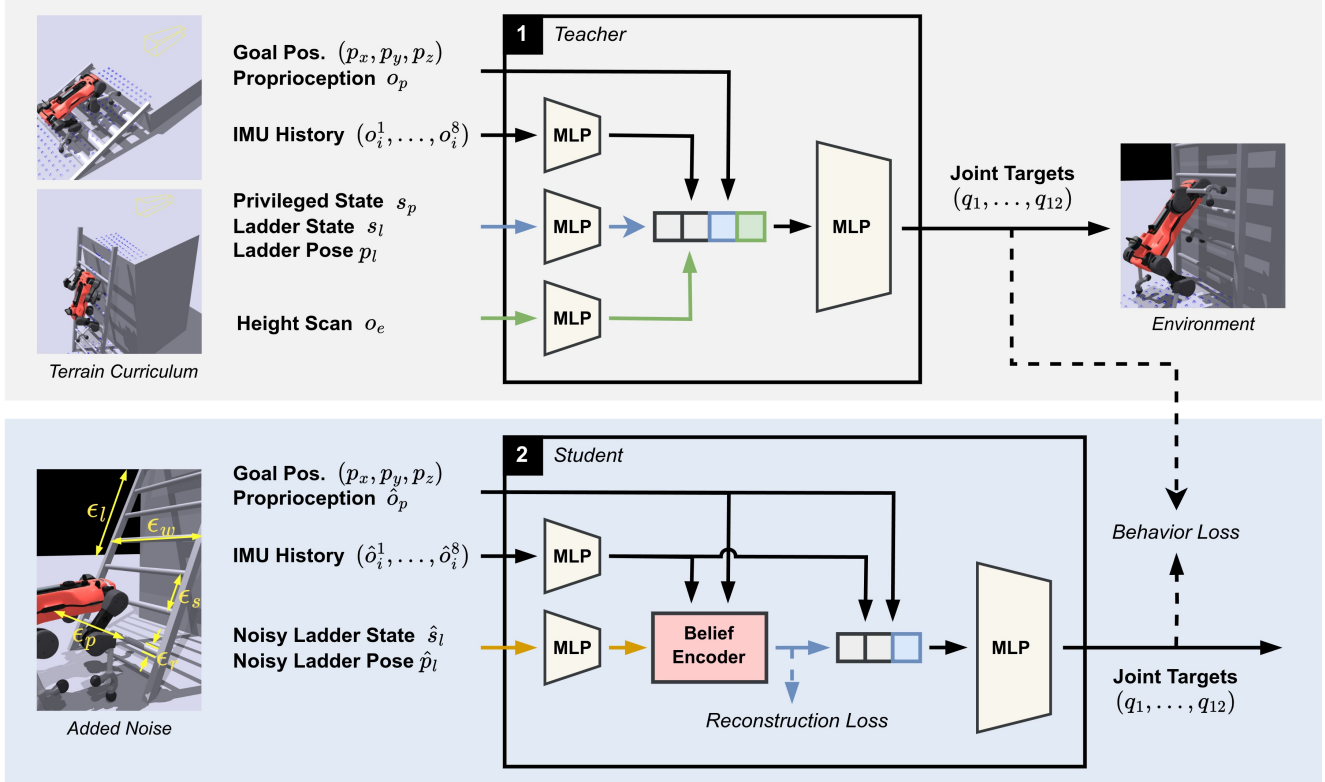


Fig. 3. Illustration of the network architecture and training pipeline. First, a teacher policy is trained in simulation with access to noiseless observations and privileged state information. Then, a student policy with a recurrent belief encoder is trained to mimic the teacher actions and reconstruct the true privileged state from noisy observations and a noisy estimate of the ladder state and pose. The student policy is the one we deploy on the actual robot hardware.

L_{radius} . The training curriculum is adaptive, and agents progress to more difficult terrains (longer, steeper) as the agent reaches earlier goals. The rungs are parameterized as elliptic cylinders with a minor axis of 2.5 cm and a major axis that decreases with increasing curriculum difficulty, down to 2.5 cm. This value was chosen such that the rungs would be smaller than the 2.75 cm opening radius of the hook. The ladders are randomly offset from the end platform up to 15 cm, with a minimum clearance for the foot as L_θ increases.

The agent is spawned in a random configuration and commanded to reach a random goal position and heading. For ladder terrains, the agent is always spawned at the base of the ladder, and the goal is always on the end platform. We randomly initialize the agent using a state from the previous episode half of the time, with additional randomization on the base and joint velocities. We find that this increases the range of states that the policy visits and improves the robustness of the final policy. Moreover, we do not sample command times, but use a dense tracking reward and allow any time up to the maximum episode length of 10 s. We find that this improves the success rate compared to prior methods [5] and allows the policy to learn emergent retry behaviors after slipping. We also apply random external forces and torques to the base and feet of the robot, and randomize the base mass and friction coefficients of the feet each episode.

TABLE I
REWARD EQUATIONS

Name	Equation
Position Tracking	$3(-\delta_{goal}(v_b \cdot \hat{p}_{goal} - v_{b,over}^2) + 1.5\delta_{goal})$
Heading Tracking	$0.5 \exp(10(\psi_{goal} - \psi_b)^2) \exp(4 p_{goal} ^2)$
Base Motion	$0.2(\exp(v_{b,z}^2) + \exp(0.5(\dot{\phi}_b^2 + \dot{\theta}_b^2)))$
Joints	$-0.001 \sum_{i=1}^{12} (0.01\ddot{r}_i^2 + \dot{q}_i^2 + 0.2\ddot{q}_i)$
Action Rate	$-0.01 \sum_{i=1}^{12} (q_{i,t}^* - q_{i,t-1}^*)^2$
Action Smoothness	$-0.01 \sum_{i=1}^{12} (q_{i,t-2}^* - 2q_{i,t-1}^* + q_{i,t}^*)^2$
Foot Slippage	$-0.25 \sum_{k \in \text{feet}} c_k v_k (1 - 0.8I(\mu_k < 0.5))$
Flat Orientation	$-\delta_f (\hat{g}_{b,x}^2 + \hat{g}_{b,y}^2)(1 + 8\delta_{goal})$
Stand Still	$-0.5\delta_{goal} \sum_{i=1}^{12} q_i^* - q_{i,0} $
Stand Still Contact	$-0.5\delta_{goal} \sum_{k \in \text{feet}} \neg c_j$
Collision	$-0.1 \sum_{k \in \text{thighs, shanks}} c_k$
Base Collision	$-c_b$

C. Student Policy Training

The student policy is trained in the same environment as the teacher, with identical initialization, domain randomization, and terrain curriculum. However, the student policy only has access to noisy versions of proprioceptive observations \hat{o}_p , IMU history \hat{o}_i^n , ladder state \hat{s}_l , and ladder pose \hat{p}_l . A small MLP encodes the noisy ladder state and pose before concatenating with the proprioceptive and latent IMU observations. This vector is passed to the belief encoder, which reconstructs the latent privileged state of the teacher,

TABLE II
SYMBOLS FOR TAB. I

Symbol	Description
v_b	Velocity of the base in base frame
$v_{b,\text{over}}$	$(\ v_b\ - 0.7) \cdot \mathbf{I}(v_b \cdot \hat{p}_{\text{goal}} > 0)$
$p_{\text{goal}}, \hat{p}_{\text{goal}}$	Vector and unit vector from base to goal in base frame
δ_{goal}	$\mathbf{I}(\ p_{\text{goal}}\ < 0.15)$
δ_f	1 if the local terrain is flat, 0 otherwise
ψ_{goal}	Yaw of the goal
ϕ_b, θ_b, ψ_b	Roll, pitch, and yaw of the base
$q_i, q_i^*, q_{i,0}$	Actual, desired, and default position of joint i
c_k	1 if body k is in contact, 0 otherwise
v_k	Velocity of body k in base frame
μ_k	Friction coefficient of body k
\hat{g}_b	Gravity direction in base frame
$\mathbf{I}(\cdot)$	Identity function

following the design of [2]. In this work, we treat the noisy ladder state and pose as exteroceptive observations. The latent privileged state is added back to the proprioceptive observations before passing to a larger MLP that produces the final actions.

The student is warm-started by copying over the matching network weights from the teacher. All other layers are randomly initialized. We collect rollouts using the student policy and compute the behavior loss by taking the mean squared error between the teacher and student actions [25]. The reconstruction loss is calculated via the L1 and L2 error between the predicted and actual privileged state. The network is trained using truncated backpropagation through time with a sequence length of 15.

A key advantage of privileged teacher-student training is that the teacher can be trained relatively quickly in the absence of noise and with knowledge of the applied disturbances. We found that the teacher struggled to learn an effective and robust policy when trained directly on student observations.

D. Simulation Setup

All simulations are performed in LeggedGym [26]. We train using 4096 parallel environments with 48 and 120 steps per batch for the teacher and student, respectively. The teacher is trained for 15,000 epochs and the student is trained for 5,000, taking around 4.5 days in total when trained on an RTX 3090. Training with the hook end-effector is around 30% slower than with the ball foot due to the additional collision bodies, which are approximated via convex decomposition.

III. RESULTS

A. Simulation Results

The student policy was evaluated in simulation across various L_θ , L_{radius} , and in the presence of noise and external disturbances. Noise was added to provide a more realistic evaluation of the robustness of the policy. During the evaluation, L_{len} was randomly sampled between 1-3 m, L_{width} between 1.0-1.25 m, and L_{space} between 27.5-32.5 cm. We

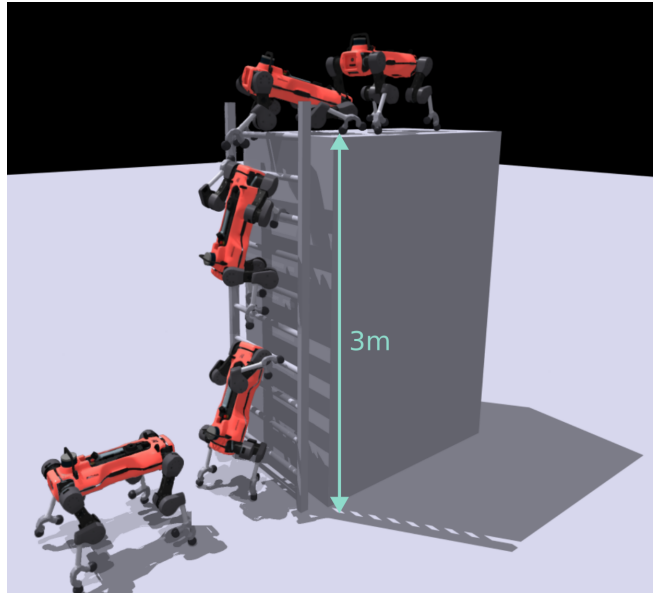


Fig. 4. A simulated robot was assessed for its ability to traverse ladders of different configurations. Shown is a composite image generated in simulation of the longest ladder tested: $L_{\text{len}} = 3$ m at $L_\theta = 90^\circ$.

sampled 50 different ladder configurations and averaged the results across 3072 agents simulated for 15 s. To more fairly compare the hook end-effector to the traditional ball-foot, the ladder rungs were made cylindrical during evaluation, rather than the elliptic cylinders used during training. An example evaluation is shown in Fig. 4.

The robot with the hooked end-effectors achieved an average 96% success rate across the configurations tested (see Fig. 5 for the success rate for each configuration). The robot successfully climbed ladders in the presence of added noise and external disturbances, such as random pushes applied to the base every 5 s, sampled from a normal distribution with a standard deviation of 1 m/s. In the case of $L_{\text{radius}} = 3.5$ cm, which is larger than the opening radius of the hook, we observed a steady drop in performance at steeper L_θ because the robot could not stabilize itself with the forelegs. As L_θ increases, the robot's applied forces switch from mostly compressive to a mix of compressive and tensile forces needed to stabilize the center of mass.

We compared the policy trained with the hook end-effector against another policy trained using the traditional ball-foot design, finding a clear performance gap across all configurations and a notable performance drop at steeper L_θ . In fact, the average success rate across all configurations was only 81% for the ball end-effector (Fig. 5). Interestingly, the performance of the ball end-effector improved with decreasing L_{radius} across all L_θ tested in simulation. We observed that the policy can exploit the small crease between the ball foot and the shank to weakly anchor the robot on the rungs at these smaller values of L_{radius} . Moreover, with decreasing L_{radius} , it became easier for the robot to maneuver its knees between the rungs, a movement strategy the policy relies on heavily in the absence of hooks.

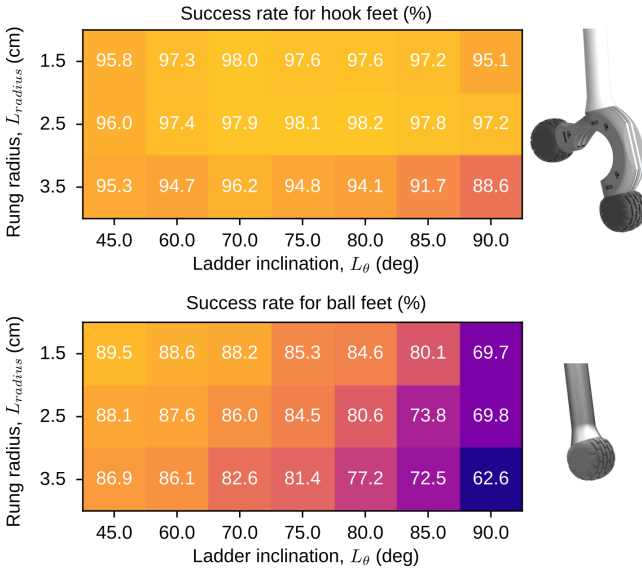


Fig. 5. Climbing success rate in simulation across various ladder inclinations and rung radii, juxtaposing performance of the ball and hooked end-effector. The agents were evaluated in the presence of noise and external disturbances.

To better understand the relative benefits of the hook end-effector, we ran noise-free simulations over the configurations in Fig. 5. The ball and hook end-effectors both yielded success rates greater than 99% in all configurations. Thus, the hook does not enable climbing in simulation *per se*, but furnishes stability to generalize over uncertainty and enables smooth and rapid climbing behavior. We see this as a critical factor for robust real-world performance.

B. Real World Results

The policy was deployed zero-shot on an ANYmal D robot (ANYbotics AG) without further fine-tuning. A motion capture system was used to estimate the ladder pose, p_l , along with L_θ . Other elements of the ladder state, s_l , were measured directly and input as scalars to the policy. In our setup, the reference ladder had parameters $L_{width} = 1$ m, $L_{len} = 1.8$ m, $L_{space} = 30$ cm (with five cylindrical rungs), and $L_{radius} = 2.5$ cm. The ladder was placed at various L_θ against a stack of wooden boxes.

Performance at varying L_θ : At L_θ values of 70° and 80° , the policy succeeded in four of four tests in each configuration. At $L_\theta = 90^\circ$, the policy succeeded in two of the three tests. During the third test at 90° , unmodeled standoffs on the base of the robot were observed to collide with the topmost rung and prevented the robot from climbing up. We decided not to proceed with further tests at 90° due to this obvious sim2real gap.

A representative sim2real experiment with a ladder at $L_\theta = 80^\circ$ is shown in Fig. 6. Snapshots of key moments highlight the close similarity between simulation and real experiments. Joint positions and environmental contacts during mounting, passing the midway point, and dismounting—culminating in a rapid roll and flick of the back right leg—closely mirror the observed simulation. The position and

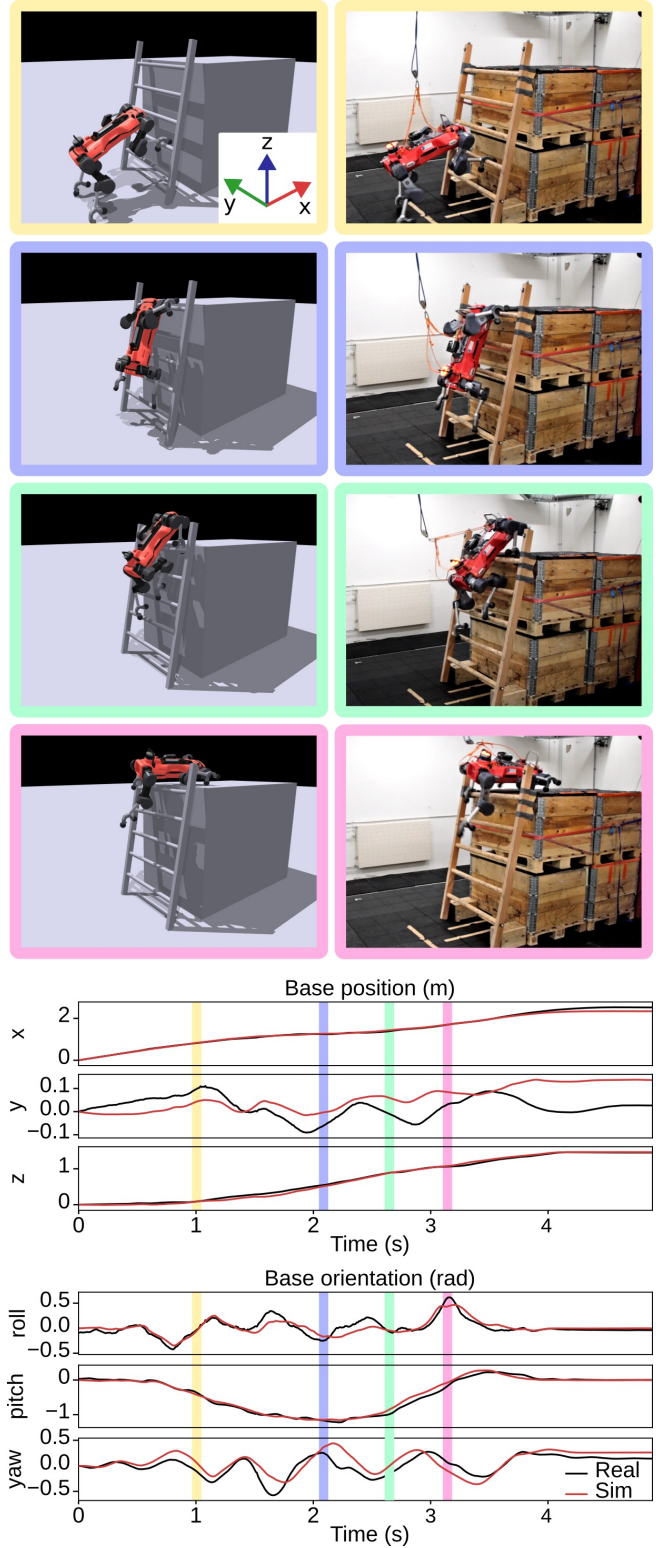


Fig. 6. Representative sim2real experiment. Key snapshots highlighted: ladder mounting, midway point, approaching the dismount, and dismount. Plots show robot base position and orientation data over time while ascending a ladder with $L_\theta = 80^\circ$. Consistency between simulation and reality is furthermore observed throughout the experiment through low deviation between Real and Sim curves.

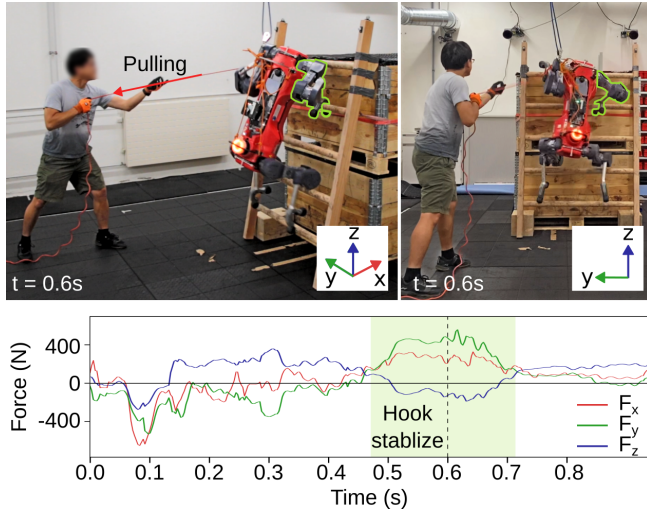


Fig. 7. The robot successfully climbs ladders even in the presence of unmodeled perturbations. Shown is an excerpt from a test at 80° with a rope tied to the robot’s front left foot. We pulled the rope at various points during the ascent. Due to the shape of the hook, the robot could successfully anchor itself, generating tension forces between its body and the rungs with its front right foot (seen as increase of F_x and F_y to the positive region of the plot and drop of F_z to the negative region).

orientation of the robot base frame between simulation and reality had an average root mean squared error of 11 cm and 0.18 rad, respectively, over the entire trajectory.

Climbing speed: We determined the robot’s average climbing speed from video footage of real experiments. We performed calculations using the time elapsed between the moment the robot first touched the ladder and the moment it fully dismounted. Over ten successfully tested ladder configurations, the average speed was 0.44 m/s (0.51 bl/s) with a standard deviation of 0.16 m/s. For context, our method yields $232\times$ faster ladder climbing speeds than the existing state-of-the-art quadruped robot in reference [16].

Unmodeled perturbations: The policy was also tested for robustness to unmodeled perturbations. In particular, we tied a rope to the front part of the chassis, back part of the chassis, or front left foot of the robot, and pulled at different moments during its ascent. Fig. 7 depicts an experiment in which the rope was tied to the robot’s front left foot. Analysis of the reaction forces over a characteristic window of time during which the robot was being pulled reveals that the robot can switch from pushing down on the rung (positive F_z) to generating tensile forces with the hook that it uses to brace itself. In other trials, the policy was found to exhibit persistent recovery and retry behaviors while being pulled from points on the base (Supplementary Video).

C. Analogy to human ladder climbing

In humans, a diagonal gait pattern is the most common method of ladder ascent. Upward thrust is generated with the hind legs, and the hands primarily maintain dynamic stability in a direction perpendicular to the ladder uprights [9], [27]. Our experimental results suggest that quadrupedal robots’

ladder ascent motions mirror this pattern, with the knees or hooked portions of hind legs generating upward thrust and the hooked forelegs primarily maintaining stability.

The duality of modes observed between humanoid and quadruped ladder climbing suggests that there exists a unifying description for the functional morphologies and control policies of humanoid and quadrupedal robots, and that they may share a large portion of the same task space. Indeed, though we humans start our lives as quadrupeds, we become primarily bipedal, sometimes reverting to a quadrupedal configuration for certain tasks (like ladder climbing).

IV. CONCLUSION

We demonstrated quadrupedal ladder climbing via a new robot end-effector design and a complementary RL-derived control policy. Our method inherently accomplishes transitions between walking and climbing locomotion modes, eliminating the need to deploy separate policies for separate modes of locomotion. The gaits and climbing behavior exhibited by the policy are completely emergent, yet interestingly, are mechanically similar to human climbing.

A comprehensive assessment of performance in simulation revealed an overall 96% success rate at climbing ladders, even with disturbances. Subsequent sim2real experiments validated that the proposed approach elicits robust and reliable policies on robot hardware. Crucially, compared to the traditional ball foot, we found that the hook end-effector furnished the stable shape needed to anchor the robot to the rungs and hang in tension with the center of mass outside of the support triangle, enabling it to traverse steeper ladders and withstand unmodeled perturbations to the base and feet. This finding emphasizes the importance of synergies between geometry and control policy for enhancing robot capabilities.

Future work will focus on realizing quadrupeds that are capable of climbing up *and down* ladders. Integrating different sensing modalities into the student training pipeline, such as depth camera images, will remove need for the motion capture system and facilitate climbing ladders at industrial sites outside of the lab. Lastly, the present hook design is not optimized, but rather chosen heuristically. There is an exciting frontier of research concerning co-optimization of morphology and control policy to accomplish multiple advanced skills with a single system.

V. ACKNOWLEDGMENTS

We would like to thank Takahiro Miki for assisting with demonstrations and brainstorming, and Fabian Tischauer for help with hardware. This work was supported by The Branco Weiss Fellowship - Society in Science, administered by ETH Zurich.

REFERENCES

- [1] Y. Li, B. Li, J. Ruan, and X. Rong, “Research of mammal bionic quadruped robots: A review,” in *2011 IEEE 5th International Conference on Robotics, Automation and Mechatronics (RAM)*, 2011, pp. 166–171.
- [2] T. Miki, J. Lee, J. Hwangbo, L. Wellhausen, V. Koltun, and M. Hutter, “Learning robust perceptive locomotion for quadrupedal robots in the wild,” *Science Robotics*, vol. 7, no. 62, p. eabk2822, 2022.

- [3] M. Shafee, G. Bellegarda, and A. Ijspeert, "Viability leads to the emergence of gait transitions in learning agile quadrupedal locomotion on challenging terrains," *Nature Communications*, vol. 15, no. 1, p. 3073, Apr. 2024.
- [4] H.-W. Park, P. M. Wensing, and S. Kim, "Jumping over obstacles with MIT Cheetah 2," *Robotics and Autonomous Systems*, vol. 136, p. 103703, Feb. 2021.
- [5] D. Hoeller, N. Rudin, D. Sako, and M. Hutter, "Anymal parkour: Learning agile navigation for quadrupedal robots," *Science Robotics*, vol. 9, no. 88, p. eadi7566, 2024.
- [6] Y. Fan, Z. Pei, C. Wang, M. Li, Z. Tang, and Q. Liu, "A review of quadruped robots: Structure, control, and autonomous motion," *Advanced Intelligent Systems*, vol. 6, no. 6, p. 2300783, 2024.
- [7] American Ladder Institute, "National ladder safety month: Ladder accidents in the home are preventable," 2024, accessed: 2024-08-13. [Online]. Available: <https://www.americanladderinstitute.org/page/NationalLadderSafetyMonthLadderAccidentsintheHomeArePreventable>
- [8] M. G. Catalano, M. J. Pollayil, G. Grioli, G. Valsecchi, H. Kolvenbach, M. Hutter, A. Bicchi, and M. Garabini, "Adaptive Feet for Quadrupedal Walkers," *IEEE Transactions on Robotics*, vol. 38, no. 1, pp. 302–316, Feb. 2022.
- [9] W. Hammer and U. Schmalz, "Human behaviour when climbing ladders with varying inclinations," *Safety Science*, vol. 15, no. 1, pp. 21–38, May 1992.
- [10] X. Sun, K. Hashimoto, S. Hayashi, M. Okawara, T. Mastuzawa, and A. Takanishi, "Stable Vertical Ladder Climbing with Rung Recognition for a Four-limbed Robot," *Journal of Bionic Engineering*, vol. 18, no. 4, pp. 786–798, Jul. 2021.
- [11] J. Vaillant, A. Kheddar, H. Audren, F. Keith, S. Brossette, A. Escande, K. Bouyarmane, K. Kaneko, M. Morisawa, P. Gergondet, E. Yoshida, S. Kajita, and F. Kanehiro, "Multi-contact vertical ladder climbing with an HRP-2 humanoid," *Autonomous Robots*, vol. 40, no. 3, pp. 561–580, Mar. 2016.
- [12] H. Yoneda, K. Sekiyama, Y. Hasegawa, and T. Fukuda, "Vertical ladder climbing motion with posture control for multi-locomotion robot," in *2008 IEEE/RSJ International Conference on Intelligent Robots and Systems*. Nice: IEEE, Sep. 2008, pp. 3579–3584.
- [13] T. Yoshiike, M. Kuroda, R. Ujino, H. Kaneko, H. Higuchi, S. Iwasaki, Y. Kanemoto, M. Asatani, and T. Koshiishi, "Development of experimental legged robot for inspection and disaster response in plants," in *2017 IEEE/RSJ International Conference on Intelligent Robots and Systems (IROS)*. Vancouver, BC: IEEE, Sep. 2017, pp. 4869–4876.
- [14] J. Luo, Y. Zhang, K. Hauser, H. A. Park, M. Paldhe, C. S. G. Lee, M. Grey, M. Stilman, J. H. Oh, J. Lee, I. Kim, and P. Oh, "Robust ladder-climbing with a humanoid robot with application to the DARPA Robotics Challenge," in *2014 IEEE International Conference on Robotics and Automation (ICRA)*. Hong Kong, China: IEEE, May 2014, pp. 2792–2798.
- [15] X. Sun, K. Hashimoto, T. Teramachi, T. Matsuzawa, S. Kimura, N. Sakai, S. Hayashi, Y. Yoshida, and A. Takanishi, "Planning and control of stable ladder climbing motion for the four-limbed Robot "WAREC"-1," in *2017 IEEE/RSJ International Conference on Intelligent Robots and Systems (IROS)*. Vancouver, BC: IEEE, Sep. 2017, pp. 6547–6554.
- [16] A. A. Saputra, Y. Toda, N. Takesue, and N. Kubota, "A Novel Capabilities of Quadruped Robot Moving through Vertical Ladder without Handrail Support," in *2019 IEEE/RSJ International Conference on Intelligent Robots and Systems (IROS)*. Macau, China: IEEE, Nov. 2019, pp. 1448–1453.
- [17] R. Grandia, F. Jenelten, S. Yang, F. Farshidian, and M. Hutter, "Perceptive Locomotion Through Nonlinear Model-Predictive Control," *IEEE Transactions on Robotics*, pp. 1–20, 2023.
- [18] J. Lee, J. Hwangbo, L. Wellhausen, V. Koltun, and M. Hutter, "Learning quadrupedal locomotion over challenging terrain," *Science Robotics*, vol. 5, no. 47, p. eabc5986, Oct. 2020.
- [19] Y. Kim, H. Oh, J. Lee, J. Choi, G. Ji, M. Jung, D. Youm, and J. Hwangbo, "Not only rewards but also constraints: Applications on legged robot locomotion," *IEEE Transactions on Robotics*, vol. 40, pp. 2984–3003, 2024.
- [20] F. Jenelten, J. He, F. Farshidian, and M. Hutter, "DTC: Deep tracking control," *Science Robotics*, vol. 9, no. 86, p. eadh5401, 2024.
- [21] C. Zhang, N. Rudin, D. Hoeller, and M. Hutter, "Learning Agile Locomotion on Risky Terrains," Nov. 2023, arXiv:2311.10484 [cs].
- [22] A. Agarwal, A. Kumar, J. Malik, and D. Pathak, "Legged locomotion in challenging terrains using egocentric vision," in *Proceedings of The 6th Conference on Robot Learning*, ser. Proceedings of Machine Learning Research, K. Liu, D. Kulic, and J. Ichnowski, Eds., vol. 205. PMLR, 14–18 Dec 2023, pp. 403–415.
- [23] J. Hwangbo, J. Lee, A. Dosovitskiy, D. Bellicoso, V. Tsounis, V. Koltun, and M. Hutter, "Learning agile and dynamic motor skills for legged robots," *Science Robotics*, vol. 4, no. 26, p. eaau5872, Jan. 2019.
- [24] Y. Liu, J. Ding, and X. Liu, "Ipo: Interior-point policy optimization under constraints," *Proceedings of the AAAI Conference on Artificial Intelligence*, vol. 34, no. 04, pp. 4940–4947, Apr. 2020.
- [25] S. Ross, G. Gordon, and D. Bagnell, "A reduction of imitation learning and structured prediction to no-regret online learning," in *Proceedings of the Fourteenth International Conference on Artificial Intelligence and Statistics*, ser. Proceedings of Machine Learning Research, G. Gordon, D. Dunson, and M. Dudík, Eds., vol. 15. Fort Lauderdale, FL, USA: PMLR, 11–13 Apr 2011, pp. 627–635.
- [26] N. Rudin, D. Hoeller, P. Reist, and M. Hutter, "Learning to walk in minutes using massively parallel deep reinforcement learning," in *Proceedings of the 5th Conference on Robot Learning*, ser. Proceedings of Machine Learning Research, A. Faust, D. Hsu, and G. Neumann, Eds., vol. 164. PMLR, 08–11 Nov 2022, pp. 91–100.
- [27] M. E. Dewar, "Body Movements in Climbing a Ladder," *Ergonomics*, vol. 20, no. 1, pp. 67–86, Jan. 1977.